Incommensurate structures investigated by X-ray studies of electropolymerised methacrylic monomer with TiO$_2$ nanoparticles

L.J. Martínez-Miranda, P. Romero-Hasler, A. Meneses-Franco & E.A. Soto-Bustamante

Published online: 12 Apr 2017.

Submit your article to this journal

Article views: 80

View related articles

View Crossmark data

Taylor & Francis
Taylor & Francis Group

Check for updates

Incommensurate structures investigated by X-ray studies of electropolymerised methacrylic monomer with TiO₂ nanoparticles

L.J. Martínez-Miranda[a], P. Romero-Hasler [b], A. Meneses-Franco[b] and E.A. Soto-Bustamante[b]

[a]Department of Materials Science and Engineering and Energy Research Center, University of Maryland, College Park, MD, USA; [b]Department of Organic Chemistry and Physical Chemistry, Faculty of Chemical and Pharmaceutical Sciences, University of Chile, Santiago, Chile

ABSTRACT

We explore the possibility of producing polymer nanocomposites with an ordered distribution of nanoparticles by using an electropolymerizable liquid crystal (LC) monomer. The nanoparticles are added to the monomer before polymerizing it. We study the polymer derived from the LC (*E*)-6-(3-hydroxy-4-(((4-octyloxy)phenyl)imino)methyl)phenoxy)hexyl methacrylate (M6R8) both pure and in the presence of 3.4 nm TiO₂ nanoparticles, at 30 wt%. This particular system is chosen since (1) the LC polymers we work with have the added advantage of having a specific orientation and structure which allows us to study its effect in the nanoparticles and (2) when considering the nanocomposite, it is polymerized with the nanoparticles included. The system is studied using grazing incidence small angle X-ray scattering and in-plane direction X-ray scattering. The polymer obtained alone appears to be tilted with respect to the surface of the substrate. The structure adopted by the nanoparticles in the nanocomposite is layered and apparently incommensurate with the polymer. It is formed through the association of the nanoparticles with the M6R8 aromatic cores during the process of electropolymerisation. This interpretation of the data is supported by the nanoparticle structures formed when the related, non-polymerizable LC, (*E*)-6-(3-hydroxy-4-(((4-octyloxy)phenyl)imino)methyl)phenoxy)hexyl isobutyrate (I6R8), is analysed. We find that for both, the pure polymer poly-((*E*)-6-(3-hydroxy-4-(((4-octyloxy)phenyl)imino)methyl)phenoxy)hexyl) methacrylate (EPM6R8) as well as the polymer with nanoparticles (EPM6R830TO), the electropolymerisation imposes a preferred growth direction of the polymer side chains, and therefore for the nanoparticle arrangement in the polymer.
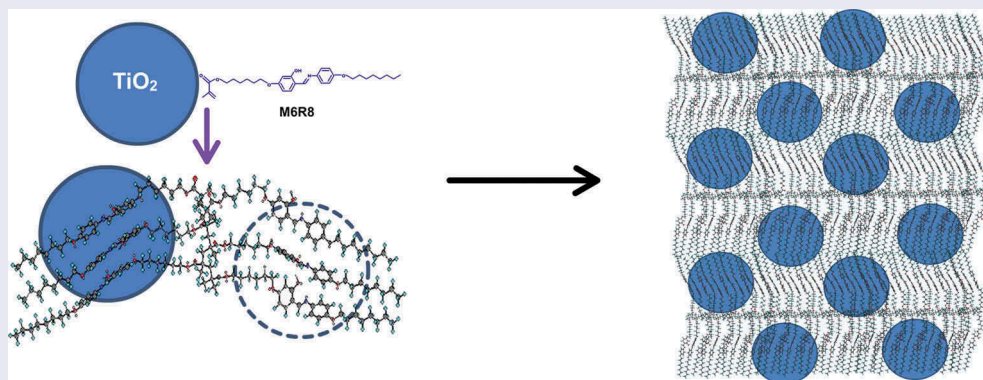
1. Introduction

Liquid crystals (LCs) are materials that combine the characteristics of a crystalline solid and an isotropic liquid. Low molar mass liquid crystalline molecules are in the order of 2–5 nm in length for the calamitics. These can be combined with nanoparticles of comparable size to form nanocomposites. Composites consisting of a mixture of nanoparticles and ordered LCs have been considered for bioengineering applications [1–5], for membrane fabrication and drug delivery [6,7], photovoltaic [8–12], photonics [13–15] and metamaterials [16,17]. These nanocomposites also serve as a model for the interfacial interactions of bilayer systems with nanoparticles. The bilayer systems are similar to those found in biological systems [5,18,19]. LCs are used also as the dispersing medium for colloidal particles, and as a flexible matrix for generating and controlling self-assembly into complex structures [20].
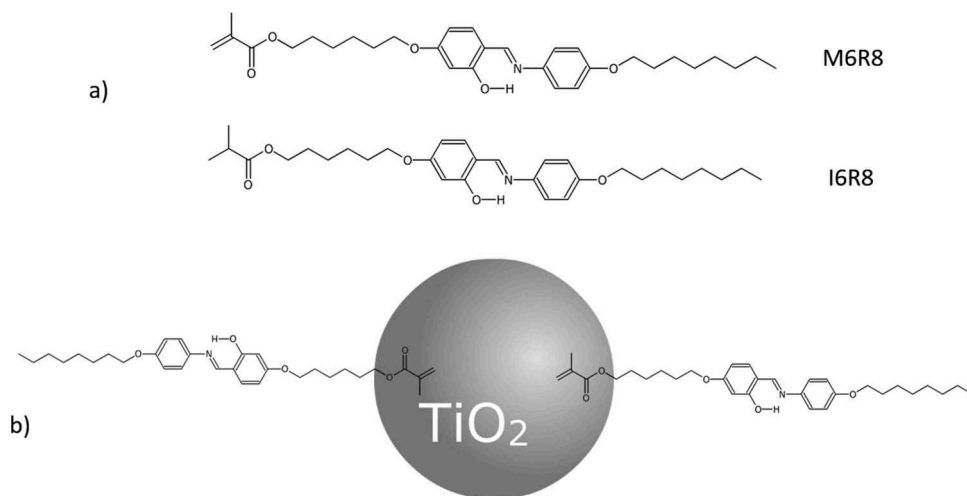
Figure 1. Sketch showing (a) the structure of M6R8 and I6R8 as well as (b) the attachment of M6R8 to the TiO$_2$ particle.

The effects of a colloidal particle in a nematic phase LC and the effects of the nematic LC on the structure the colloids form have been studied extensively [20–32]. On the other hand, interactions of nanoparticles with smectics have not been studied as widely [10,11,33–38]. Previously, we have shown that the ordering of bulk smectic LCs is influenced by the presence of functionalized nanoparticles [10,11,35,39]. The influence of other materials, such as polymers on the orientation the nanoparticle adopts, has also been reported [6,7,40–45].

In the samples used in this study, the nanoparticles have been prepared such that they are terminated in hydroxy groups and form hydrogen bonds [46–49] with the LCs. The hydrogen bonds can be disturbed through the process of electropolymerisation [50,51]. We are not aware of any groups that are developing a strategy that includes the nanoparticles in the monomer nanocomposite before a polymeric matrix is formed and uses electropolymerisation to align both the resulting polymer and the nanoparticles. We can control the structure and the orientation in space, both for the LC polymers and the nanocomposites in ways that have not been explored before by using both of these methods.

The organised structures that we obtain offer another alternative to the development of applications, particularly photovoltaic applications. We studied the polymer nanocomposites for their potential applications in photovoltaics. It is well known that a polymer has a higher mechanical integrity compared with low molar mass molecules due to the polymeric network. In addition, a LC polymer has the advantage of being a more ordered system as compared to the more commonly used amorphous polymers.

Previously, we have investigated LC–nanoparticle interactions of two different monomeric LCs combined with TiO$_2$ to form a nanocomposite [52]. The LCs are M6R8 and I6R8, which are shown in Figure 1(a). The two low molar mass compounds differ in the final group at the end of one of the carbon chains [52]. We have a double bond conjugated with a carbonyl group or methacrylate group in the case of M6R8. We believe that the nanoparticles locate themselves at the layer interface where the methacrylic groups are present.

The conjugated double bond seems to be energetically more favourable to form hydrogen bond interactions with the TiO$_2$, most probably due to structural considerations, in this case. The electron availability in the carbonyl moiety is enhanced due to the presence of the double bond, which in turn will interact with the OH groups present at the surface of the nanoparticles. This is shown in Figure 1(b). The double bond itself can also interact with the electrophilic surface of the nanoparticles rich in titanium atoms, in a sort of π-complex interaction. The carbon–carbon double bond for I6R8 is missing, and this group is then an isobutyric ester. In the case of I6R8 with TiO$_2$ particles, the observed decrease of the enthalpy and therefore the phase stability can be understood as a distribution of more nanoparticles at the aromatic cores since no places are allowed at the layer interfaces, due to the absence of methacrylic groups.

The 30-wt% concentration of TiO$_2$ yields the most organised nanocomposite for the monomer M6R8 [52]. This result has been previously observed with ZnO in 8CB [10,11,35].

We have observed that in addition to obtaining the alignment of the polymer by the process of electropolymerisation, we obtain the alignment of the nanoparticles

because of the electropolymerisation in the study of the polymeric sample EPM6R830TO. The structures obtained with the nanoparticles in the nanocomposite are incommensurate. This is an ongoing programme that combines LCs and polymer LCs and that seeks to promote the formation of organic–inorganic systems of molecular diodes where a strict molecular distribution must be achieved.

This paper presents a series of X-ray scattering studies taken in order to confirm the alignment of the pure polymer and polymer nanocomposite, to confirm the orientation of the interaction of the TiO_2 nanoparticle with the polymer and to determine the ordering of the nanoparticle with respect to the polymer and the substrate. Our results are quite promising about the order we are achieving in our structured nanocomposites.

2. Experimental

2.1 Materials

The monomer M6R8 is obtained using a procedure described elsewhere [52–54]. The LC properties correspond to a C-54.7°C–SmC-80°C–SmA-97.0°C–I [55]. The synthesis of I6R8 will be reported elsewhere, and it has a phase transition temperature C-62.7°C–SmC-89.4°C–SmA-98.3°C–I. The temperatures are C-55.1°C–SmC-68°C–SmA-97.1°C–I, in the case of M30, a nanocomposite of M6R8 with 30 wt%. TiO_2 Np. For the corresponding I6R8 nanocomposite (I30), the phase transitions are C-61.8°C–SmC-70°C–SmA-97.3°C–I [52].

The nanocomposites are prepared taking about 150 mg of the liquid crystalline matrix dissolved in DMF. The required amounts of a suspension of nanoparticles are measured to obtain a mixture of 30 wt%. The solutions are subjected to ultrasound for about 30 min and dried under vacuum at 80°C, for a quick but gentle solvent evaporation.

In Ref. [52], the characterisation of TiO_2 nanoparticles was carried out. Particle size was quite homogeneous, at around 3–4 nm, or in our case, approximately 3.4 nm. Figure 2 shows a HR-TEM of a 5-nm nanoparticle in the left top side of the figure. Besides, it is a diffraction pattern which shows numerous rings because the beam of electrons included a large number of particles with different orientations. It shows rings of spots corresponding to the random orientation of the nanoparticles. The bottom picture is a low-resolution image of TiO_2 showing the size uniformity of the particles.
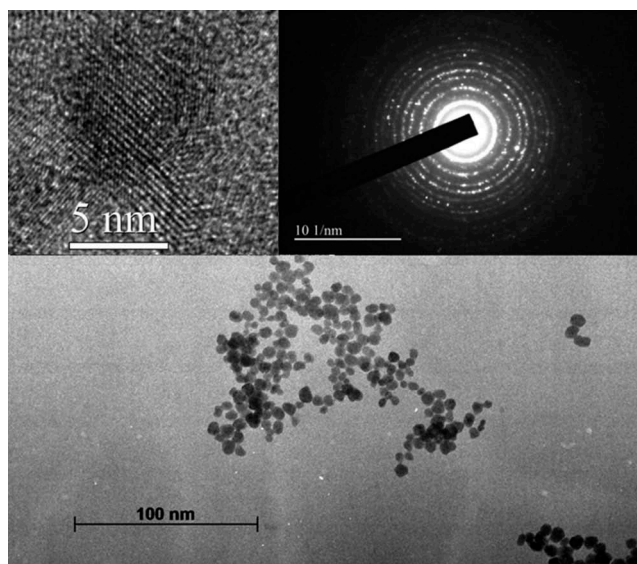

Figure 2. TEM images for TiO_2. Upper images: HR-TEM image of a single particle and an electron diffraction pattern for the particles. Lower image: a low-resolution TEM showing the relative uniformity of the particles.

2.2 Electropolymerisation

The polymer EPM6R830TO was obtained by filling INSTEC cells with the nanocomposite via capillary action in the isotropic phase. The cells used (INSTEC) are comprised indium–tin–oxide electrodes, covered with polyimide with antiparallel planar alignment layers. The cell gap is of 6.8 μm. The electropolymerisation was conducted by applying a DC field of about 100 V at 120°C for about 1 h.

2.3 X-ray analysis

The electropolymerised polymer obtained from M6R8 without nanoparticles (EPM6R8) was studied using the small angle X-ray scattering facility at the University of São Paulo, Brazil. A Xenocs Xeuss system was used, which consists of a GeniX3D beam delivery system with a Cu anode X-ray tube (λ = 1.5419 Å), a collimation composed of two scatterless slits and a Pilatus 300K detector (Dectris, Baden, Switzerland). The beam has a square cross section of 0.8 × 0.8 mm^2. The beam centre correction and the sample to detector distance of 83.5 cm were measured using silver behenate [56].

The X-ray experiments on the polymer LC-nanoparticle (EPM6R830TO) were performed using a Rigaku rotating anode with a Cu (1.54 Å) source, and a bent graphite monochromator with a resolution of $\Delta q = 0.012q_0$ (Å^{-1}), operating at 50 kV and 100 mA, where $q_0 = 2\pi/1.5442$ [57].

The polymer nanocomposite, prepared as described above, was measured on an opened cell placed along the
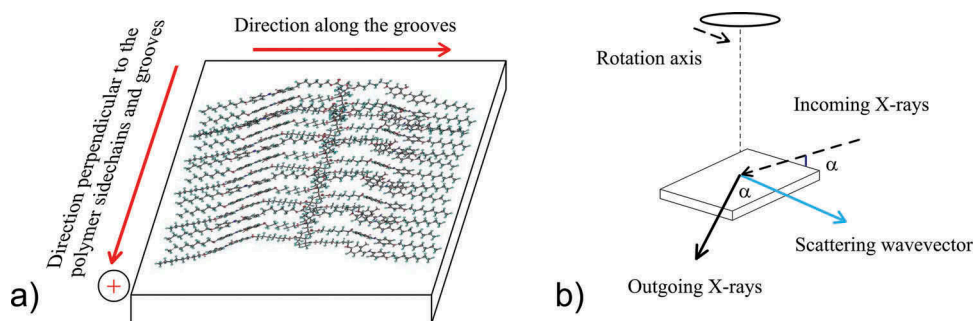
Figure 3. (Colour online) (a) Definition of directions used to study the polymer nanocomposites shown from the top and from the side view. The nanoparticles are not drawn for clarity; (b) geometry of the parallel X-ray scattering: the two directions shown above are aligned such that the scattering wavevector direction coincides with the direction along the grooves or perpendicular to it.

direction of the rubbed polyimide grooves (see Figure 3 (a)). The sample was then rotated 90° with respect to the aforementioned direction in order to observe if there was any order along this direction. This last direction is called the perpendicular (perp) direction in the discussion that follows. Figure 3(a) sketches both directions. The X-ray measurements were taken with the substrate in what is called the parallel geometry, sketched in Figure 3(b). This geometry is similar to the one used in grazing incidence X-ray scattering (GIXS), except it accepts a wider angular distribution. The angle α, shown in Figure 3(b) also, covers angles beyond the critical angle [39,57] which corresponds to an α of 0.12° for most organic materials [58]. The X-ray scans are analysed by taking a background with a clean substrate and subtracting this background from the signal.

2.4 Other analysis techniques

The electropolymerisation requires the monomers or composites to be confined in a 6.8-μm thick sandwich glass cell. The polymerisation takes place mostly at the negative electrode surface and the structural characterisation must be performed on the glass substrate to determine the direction of the orientation of the polymer and the resulting structure adopted by the nanoparticles. The amount of material is too small to obtain adequate results using complementary techniques such as NMR. Other techniques require the material to be released from the substrate, which may mean a loss of the aforementioned desired structural properties.

3. Results

The polymer in both cases is obtained through the process of electropolymerization [50,51], mentioned above. Electro-polymerisation is carried out in the

isotropic state of the monomer and the monomers are aligned with the direction of the polyimide grooves. The process of electro-polymerization by itself makes the preparation of nanocomposites easier by including the nanoparticles inside the monomeric matrix, in this case, 30 wt% TiO_2.

The results for the polymer with nanoparticles (EPM6R830TO) were compared to the results obtained when the polymer is grown without them (EPM6R8). The polymer structure was studied using the grazing incidence small angle X-ray scattering (GISAXS) technique, using a grazing incidence angle of 0.2° on uncovered glass samples as mentioned in Section 2. The samples were placed in the direction along the grooves, as shown in Figure 3(a).

Comparison of Figure 4 and the lower panel of Figure 5 shows the formation of polymer peaks. Only two are visible in Figure 5 lower panel. The polymer
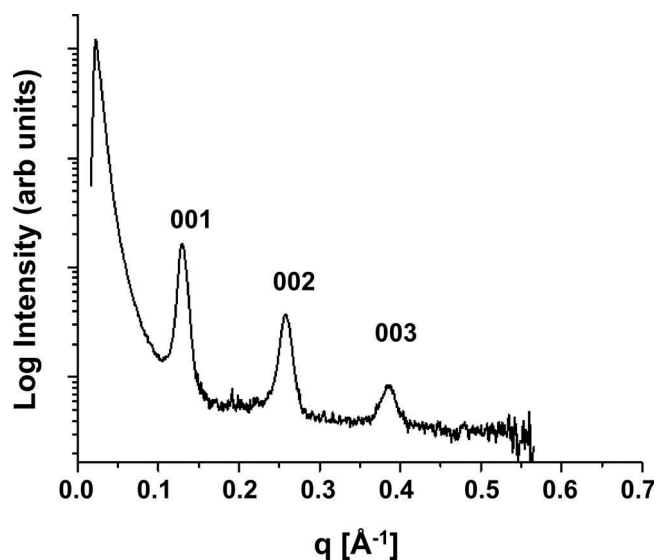

Figure 4. GISAXS scan for the EPM6R8 polymer showing the first three reflections.
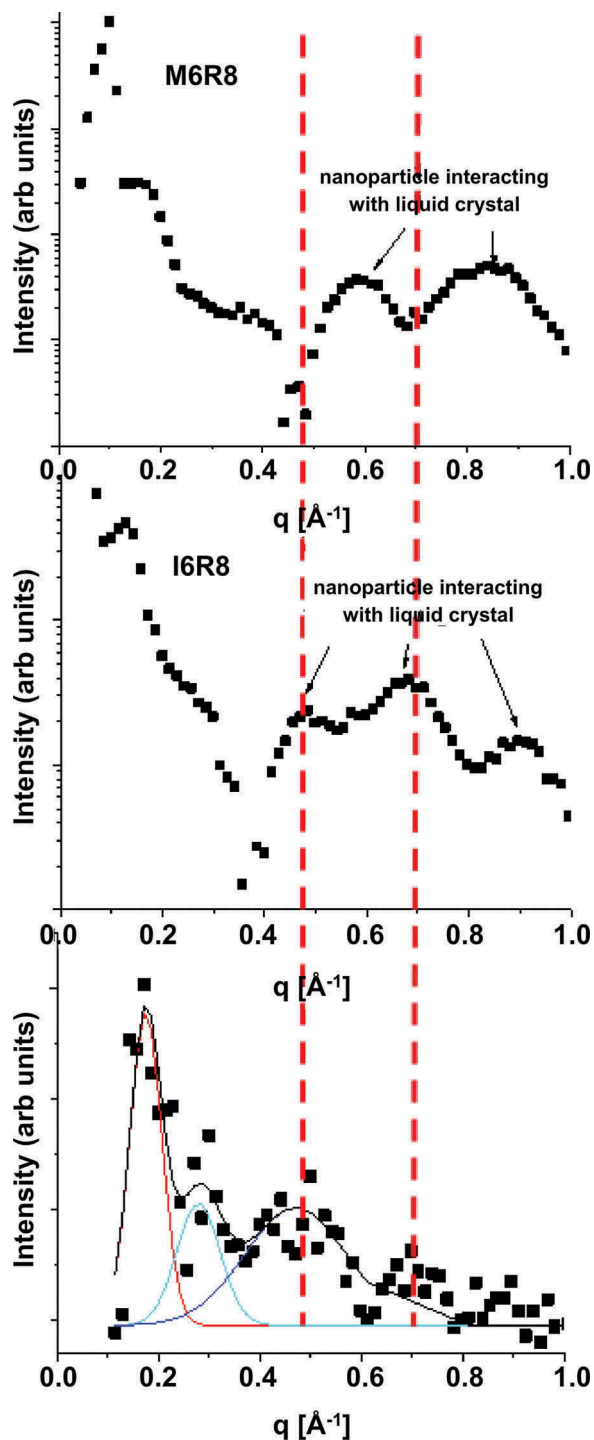
Figure 5. (Colour online) A comparison between the monomeric composites M6R8 (M30 – top panel) and I6R8 (I30 – middle panel) with the polymer produced from M6R8 (EPM6R830TO – lower panel). All samples have a 30-wt% concentration of TiO_2. Notice that the peaks at about 0.5, 0.7 and 0.9 $Å^{-1}$ between I6R8 and the polymer coincide.

longer than what is expected. The results for the polymer–nanoparticle nanocomposites were compared to the results from the two monomer LCs–nanoparticle nanocomposites, the M6R8 and the I6R8. We include the results for I6R8 because this sample does not polymerise, and we know how it interacts with the TiO_2. As mentioned before, the TiO_2 is located at the Schiff base central group for I6R8, whereas for M6R8, the preferred position for TiO_2 is at the methacrylate group [52]. We find that the peaks associated with the nanoparticle–LC interaction for the nanocomposite EPM6R830TO are similar to those of the monomeric nanocomposite of TiO_2 with I6R8, as can be observed if we compare the last two panels of Figure 5. This provides evidence that the nanoparticles migrate from the edge of the molecule to the centre group, as sketched in Figure 6. The migration is a consequence of the polymerisation of the M6R8 monomer. The polymerisation happens through the methacrylic groups where the TiO_2 groups are located.

We consider now the fact that the signal from the nanoparticle is small and noisy, as can be observed in Figure 7. Taking into account the well-known density of rutile and anatase and that our TiO_2 samples are a mixture of both structures, we may assume an average density of 4 g/cm^3. For an average size of the TiO_2 Np of 3.4 nm, we can consider that roughly each Np has a volume of 20.6×10^{-21} cm^3. With these data, it is possible to find out the amount of Np for the 30 wt%, if we also consider that the diameter of the nanoparticle amounts to at least five side chains in the polymer. It gives a ratio of 1 TiO_2 Np per 50 polymer ensembles, which is quite far away from an ideal ratio of 1:1.

The nanoparticle shown in Figure 6 as a cut line is because the concentration of the nanoparticle is 30 wt% and not 1:1. Thus, the second nanoparticle may be there or not, depending on how the nanocomposite is mixed and how the nanoparticles migrate to the centre group. This explains in part why the signal tends to be noisy.

Another possible explanation for the peaks being noisy is the localisation of the nanoparticles due to phase separation [57]. The nanoparticles accumulate mostly in the defects exhibited by the LC after some time. When the process of electropolymerisation occurs, the defects disappear since the sample is taken into the isotropic and the nanoparticles are free to migrate. This process is limited by the formation of the LC polymer whose branching represents a steric hindrance to the advancement of the nanoparticles. Thus, the structure of the nanoparticles can be very
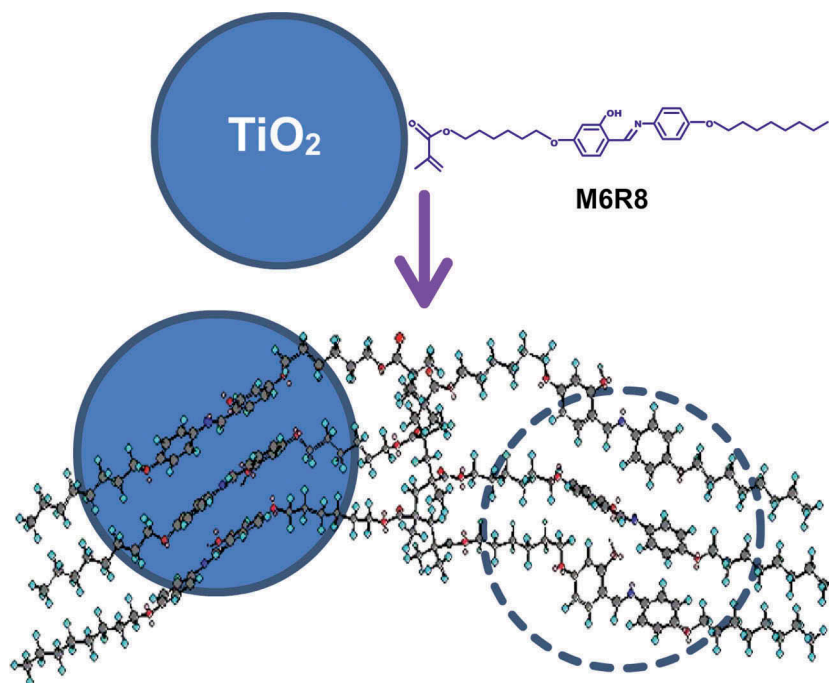
alone was found to be at an angle with respect to the surface of 38.7° calculated from the 001 reflection in Figure 4. The polymer–nanoparticle system, on the other hand, seems to be completely lying down and

Figure 6. (Colour online) Sketch showing the migration of the TiO₂ particle while the polymer is formed.

well ordered locally but not globally in the sample, which gives again a very noisy signal. This means that a very well-organised structure can happen locally, separated by a distance that is much larger than the atomic distance, in the order of micrometres. This signal is noisy and wide at all q values. This can explain why lower q peaks are not observed. The signal coming from the nanoparticles structure will be very small compared to the more ordered polymer signal. The lower the angle, the closer to the polymer peak the

peak from the nanoparticles will be. We look at the signal we observe in detail now.

We show in Figure 7 the results of X-ray measurements taken both along the direction of the grooves (see Figure 7(a)) and perpendicular to it (see Figure 7(b)) for three different temperatures that correspond to the crystalline (21°C), the smectic C (56°C) and the smectic A (73°C) of the parent monomer, M6R8[52]. The scans taken along the groove direction show an extra peak close to $q = 0.47$ Å^{-1}, as seen in Figure 7(a). This peak corresponds to one of the peaks designated
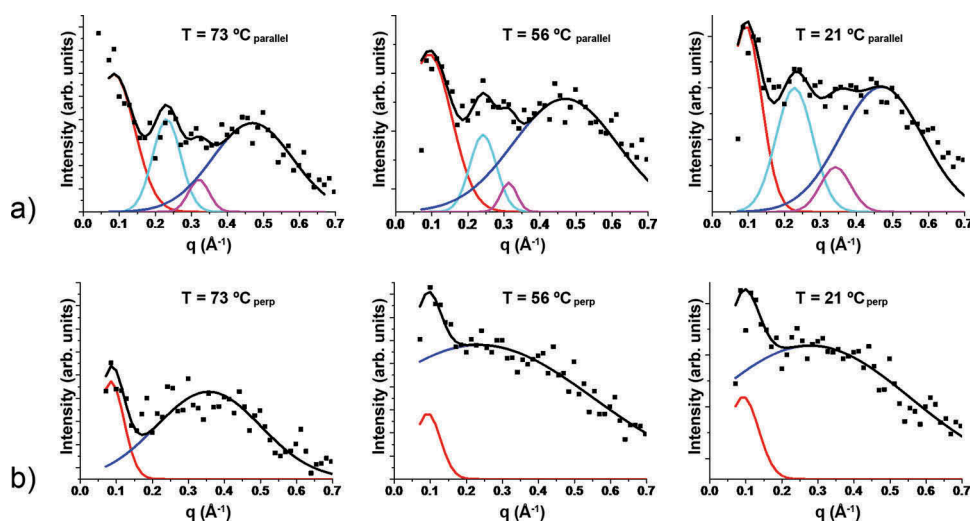

Figure 7. (Colour online) X-ray scans showing the structure of EPM6R830TO in the direction (a) parallel to the polyimide grooves and (b) perpendicular to this direction. The lines are fits to Gaussians.
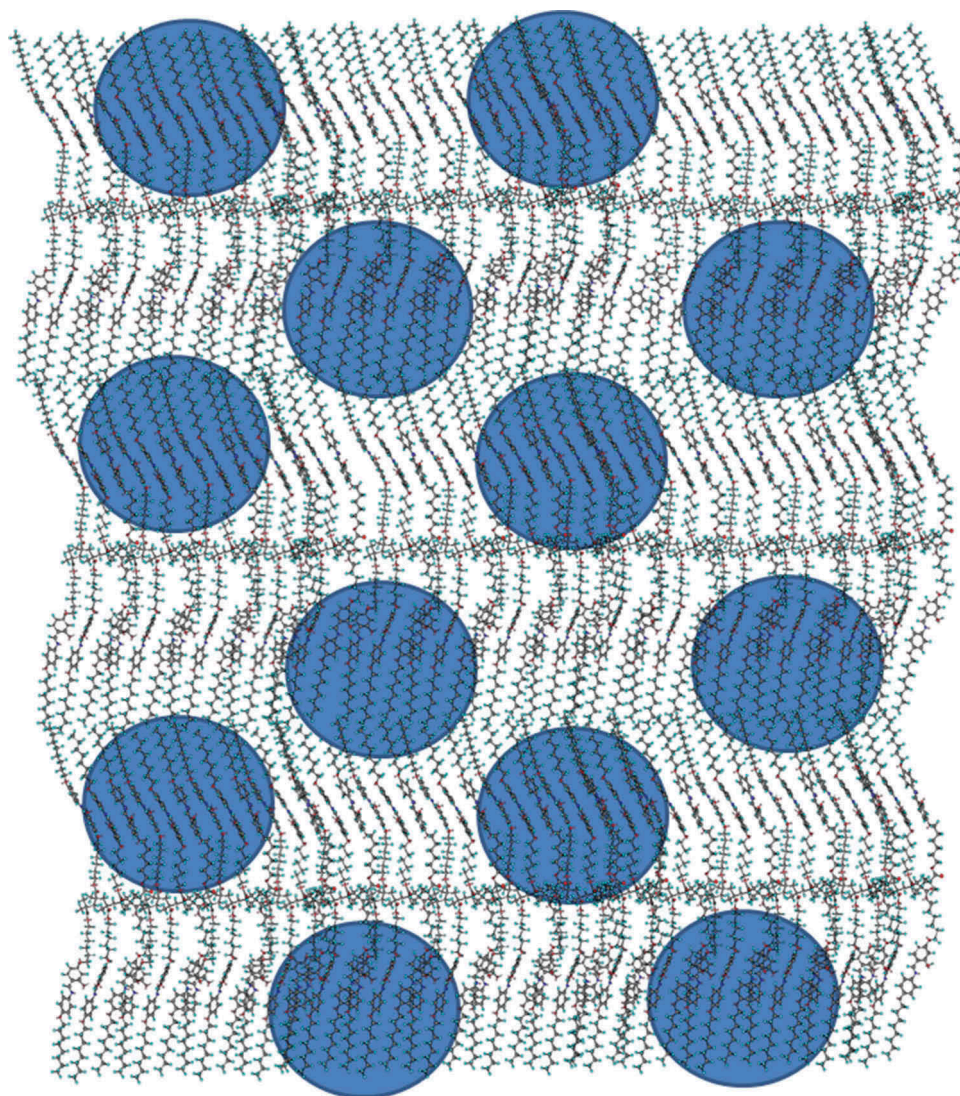
Figure 8. (Colour online) A possible structure derived from the X-ray scans shown. All nanoparticles are presented for clarity.

for the nanoparticle interacting with the LC in Figure 5. The scans along both directions exhibit a peak corresponding to the polymer peak at low angles, as seen in Figure 7.

The scans along the direction of the grooves (Figure 7(a)) exhibit more ordered peaks in the region of $0.25 \leq q \leq 0.33$ Å^{-1}. These peaks correspond to the polymer peaks shown in Figure 4. The scans designated as 'perp' to these have a very disordered peak centred at $q \sim 0.25$ Å^{-1} with a Δq that varies between 0.3 and 0.6 Å^{-1}, with the more disordered being in the smectic C phase and the more ordered being in the smectic A phase. No higher order peaks are observed, even though we note a small peak at the position of the (0 0 1) of the polymer. See Figure 7(b) and note that the polymer (0 0 1) peak is smaller than the value for the polymer peak given in Figure 7(a), even though it appears comparable. This is because of the sum of this peak with the

very wide peak mentioned above. These results show that for the polymer nanocomposite, the electropolymerisation imposes a preferred direction.Figure 4

The electropolymerisation imposes also a preferred direction to the nanoparticle's structure, as seen in Figure 7(a) compared to Figure 7(b). The figure shows a peak at around 0.47 Å^{-1}, which is the same one attributed to the interaction of the LC or its corresponding polymer with the nanoparticles in Figure 5 (EPM6R830TO). This wide peak has a value that varies between 0.2 and 0.4 Å^{-1} with a Δq that varies between 0.2 and 0.3 Å^{-1} for all samples presented in Figure 7(b). This peak is more disordered than the polymer peaks and does not coincide with any of the reflections of the polymer structure.

The structure of the nanoparticle appears to be incommensurate with the structure of the polymer [59], probably because of the size and shape of the

nanoparticles. We analyse more closely the peak observed at 0.47 $Å^{-1}$. This peak corresponds to a separation of 13.4 Å. There is no evidence from Figure 5 or Figure 7(a) that there is a lower angle reflection. The qs corresponding to the polymer peaks in Figure 7(a) do not show an underlying wide peak that would correspond to a lower q peak. We cannot access any reflection below 0.09 $Å^{-1}$, and hence we cannot say if there is a lower q peak. The nanoparticle must rest at the centre of the side chain molecules, as seen in Figure 5. The theoretical side chains lengths may vary between 33.95 and 37.1 Å. The nanoparticle size is about 34 Å, so this direction corresponds to a scattering angle of at least 67°. This means that the distribution of the nanoparticles is probably as sketched in Figure 8, with the nanoparticles alternating positions in the side chains of the polymer. This can be understood if we consider that the nanoparticles are slightly larger than the side chains of the polymer and accommodate this difference adopting the mentioned oblique structure. The length in the direction perpendicular to the direction of the grooves is at least 31.30 Å, which corresponds to $q = 0.201$ $Å^{-1}$. This is the maximum value of q expected, which will be reached if the nanoparticles touch. We do not expect higher order peaks to appear since the peak is very disordered. Therefore, we believe that the value for the very wide peak observed along the perp direction is probably due to the disordering of the polymer in that direction (see Figure 7(b)).

The structure the nanoparticles adopt is an oblique one that does not correspond to a 2D face centred rectangular structure because of the preferred direction of the polymer backbone and the fact that this backbone cuts the centred rectangle. Figure 8 shows a sketch of how this structure may look. The structure is then a lamellar one bounded by the polymer chains, which is consistent with the structure predicted for nanoparticles with very small coverage of the functionalisation or none in the nanoparticles [16], and observed with mixtures of nanoparticles and liquid crystalline polymers [46,60]. Because none of the q values correspond to the qs of the polymer, this structure can be considered an incommensurate one.

The nanoparticles are of comparable size to the side chains of the polymer and force them to lie flat and extend to their maximum size, which is theoretically 37.1 Å. The layer thickness exceeds the theoretical 62 Å for a completely extended side chain EPM6R8. The value for the length of the polymer is 65 Å for the samples studied at 21 and 56°C. This value is somewhat larger than 62 Å and it is much larger than the 48.3 Å reported for EPM6R8 and presented in Figure 4. We note that at 73°C, the distance is of 74 Å, the temperature corresponding to the smectic A in the parent LC monomer M6R8, which means that the polymer appears more elongated than expected for the polymer alone and at lower temperatures. We believe the decrease in viscosity due to the higher temperature increases to some extent the diffusion of the nanoparticles thus causing the increase in the interlayer distance.

4. Conclusions

We have studied the polymer formed from the monomer M6R8 both in pure form and as a nanocomposite with 30 wt% of TiO_2 nanoparticle of average size 3.4 nm (34 Å), grown by electropolymerisation. The electropolymerisation imposes a specific direction of growth of the polymer in both cases. The polymer grown in pure form appears to be at an angle with respect to the surface of the substrate. We have observed that the interaction of the nanoparticle and the polymer EPM6R830TO is similar to that of the monomer I6R8 and the nanoparticle, which suggests that the nanoparticle migrates as the polymer is formed. The size of the TiO_2 particle seems to force the polymer to be flat with the surface of the substrate to relax and expand on it. This effect is observed at three different temperatures characteristic of the crystal, the smectic C and the smectic A phases of the parent monomer M6R8. Finally, the structure of the nanoparticles seems to be incommensurate with the structure of the polymer and aligned by the electropolymerisation method. It is lamellar and oblique in nature. This can be understood if the nanoparticles group themselves through the polymer and the oblique nature appears if the slight difference in size between the side chains of the polymer and the nanoparticles is taken into account.

Disclosure statement

No potential conflict of interest was reported by the authors.

Funding

ORCID

P. Romero-Hasler http://orcid.org/0000-0002-9211-2514

References

[1] Goodby JW. Liquid crystals and life. Liq Cryst. 1998;24:25–38.

[2] Pankhurst QA, Connolly J, Jones SK, et al. Applications of magnetic nanoparticles in biomedicine. J Phys D: Appl Phys. 2003;36:R167–R81.

[3] Stewart GT. Liquid crystals in biology - I. Historical, biological and medical aspects. Liq Cryst. 2003;30:541–557.

[4] Lagerwall JPF, Scalia G. A new era for liquid crystal research: applications of liquid crystals in soft matter nano-, bio- and microtechnology. Curr Appl Phys. 2012;12:1387–1412.

[5] Taylor JW, Kurihara LK, Martinez-Miranda LJ. Interaction of a bi-molecular liquid crystal film with functionalized nanoparticles. Appl Phys Lett. 2012;100:173115.

[6] Isa L, Calzolari DCE, Pontoni D, et al. Core-shell nanoparticle monolayers at planar liquid-liquid interfaces: effects of polymer architecture on the interface microstructure. Soft Matter. 2013;9:3789–3797.

[7] Calzolari DCE, Pontoni D, Deutsch M, et al. Nanoscale structure of surfactant-induced nanoparticle monolayers at the oil-water interface. Soft Matter. 2012;8:11478–11483.

[8] Yuan K, Li F, Chen L, et al. Liquid crystal helps ZnO nanoparticles self-assemble for performance improvement of hybrid solar cells. J Phys Chem C. 2012;116:6332–6339.

[9] Chen W, Chen YW, Li F, et al. Ordered microstructure induced by orientation behavior of liquid-crystal polythiophene for performance improvement of hybrid solar cells. Sol Energy Mater Sol Cells. 2012;96:266–275.

[10] Martinez-Miranda LJ, Traister KM, Melendez-Rodriguez I, et al. Liquid crystal-ZnO nanoparticle photovoltaics: role of nanoparticles in ordering the liquid crystal. Appl Phys Lett. 2010;97:223301.

[11] Branch J, Thompson R, Taylor JW, et al. ZnO nanorod-smectic liquid crystal composites: role of ZnO particle size, shape, and concentration on liquid crystal order and current-voltage properties. J Appl Phys. 2014;115:164303.

[12] Weickert J, Dunbar RB, Hesse HC, et al. Nanostructured Organic and Hybrid Solar Cells. Adv Mater. 2011;23:1810–1828.

[13] Rodarte AL, Nuno ZS, Cao BH, et al. Tuning quantum-dot organization in liquid crystals for robust photonic Applications. ChemPhysChem. 2014;15:1413–1421.

[14] Rodarte AL, Shcherbatyuk GV, Shcherbatyuk L, et al. Dynamics of spontaneous emission of quantum dots in a one-dimensional cholesteric liquid crystal photonic cavity. RSC Adv. 2012;2:12759–12763.

[15] Rodarte AL, Gray C, Hirst LS, et al. Spectral and polarization modulation of quantum dot emission in a one-dimensional liquid crystal photonic cavity. Phys Rev B. 2012;85:035430.

[16] Draper M, Saez IM, Cowling SJ, et al. Self-assembly and shape morphology of liquid-crystalline gold metamaterials. Adv Funct Mater. 2011;21:1260–1278.

[17] Pratibha R, Park K, Smalyukh II, et al. Tunable optical metamaterial based on liquid crystal-gold nanosphere composite. Opt Express. 2009;17:19459–19469.

[18] Roiter Y, Ornatska M, Rammohan AR, et al. Interaction of lipid membrane with nanostructured surfaces. Langmuir. 2009;25:6287–6299.

[19] Roiter Y, Ornatska M, Rammohan AR, et al. Interaction of nanoparticles with lipid membrane. Nano Lett. 2008;8:941–944.

[20] Soule ER, Milette J, Reven L, et al. Phase equilibrium and structure formation in gold nanoparticles-nematic liquid crystal composites: experiments and theory. Soft Matter. 2012;8:2860–2866.

[21] Ravnik M, Zumer S. Landau-de Gennes modelling of nematic liquid crystal colloids. Liq Cryst. 2009;36:1201–1214.

[22] Musevic I, Skarabot M, Tkalec U, et al. Two-dimensional nematic colloidal crystals self-assembled by topological defects. Science. 2006;313:954–958.

[23] Mondain-Monval O, Dedieu JC, Gulik-Krzywicki T, et al. Weak surface energy in nematic dispersions: saturn ring defects and quadrupolar interactions. Epj B. 1999;12:167–170.

[24] Mondiot F, Chandran SP, Mondain-Monval O, et al. Shape-induced dispersion of colloids in anisotropic fluids. Phys Rev Lett. 2009;103:238303.

[25] Loudet JC, Barois P, Poulin P. Colloidal ordering from phase separation in a liquid-crystalline continuous phase. Nature. 2000;407:611–613.

[26] Musevic I. Nematic colloids, topology and photonics. Philos Trans R Soc London Ser. 2013;371:20120266.

[27] Melle M, Schlotthauer S, Mazza MG, et al. Defect topologies in a nematic liquid crystal near a patchy colloid. J Chem Phys. 2012;136:19703.

[28] Soule ER, Rey AD. Hedgehog defects in mixtures of a nematic liquid crystal and a non-nematogenic component. Soft Matter. 2012;8:1395–1403.

[29] Loudet JC, Barois P, Auroy P, et al. Colloidal structures from bulk demixing in liquid crystals. Langmuir. 2004;20:11336–11347.

[30] Fukuda J, Stark H, Yokoyama H. Friction drag of a spherical particle in a liquid crystal above the isotropic-nematic transition. Phys Rev E Stat Nonlin Soft Matter Phys. 2005;72:021701.

[31] Stark H, Ventzki D. Non-linear Stokes drag of spherical particles in a nematic solvent. Europhys Lett. 2002;57:60–66.

[32] Stark H. Saturn-ring defects around microspheres suspended in nematic liquid crystals: an analogy between confined geometries and magnetic fields. Phys Rev E Stat Nonlin Soft Matter Phys. 2002;66:032701.

[33] Milette J, Relaix S, Lavigne C, et al. Reversible long-range patterning of gold nanoparticles by smectic liquid crystals. Soft Matter. 2012;8:6593–6598.

[34] Patricio P, Tasinkevych M, Da Gama MMT. Colloidal dipolar interactions in 2D smectic-C films. Epj E. 2002;7:117–122.

[35] Martinez-Miranda LJ, Taylor JW, Kurihara LK. Liquid crystals nanocomposites for photovoltaic applications: structural properties. Mol Cryst Liq Cryst. 2014;594:100–104.

[36] Meneses-Franco A, Trujillo-Rojo VH, Soto-Bustamante EA. Synthesis and characterization of pyroelectric nanocomposite formed of BaTiO3 nanoparticles and a smectic liquid crystal matrix. Phase Transitions. 2010;83:1037–1047.

[37] Cordoyiannis G, Gyergyek S, Rožič B, et al. The effect of magnetic nanoparticles upon the smectic-A to smectic-C* phase transition. Liq Cryst. 2016;43:314–319.

[38] Rasna MV, Cmok L, Evans DR, et al. Phase transitions, optical, dielectric and viscoelastic properties of colloidal suspensions of BaTiO3 nanoparticles and cyanobiphenyl liquid crystals. Liq Cryst. 2015;42:1059–1067.

[39] Martinez-Miranda LJ, Kurihara LK. Interaction and response of a smectic-A liquid crystal to a nanometer particle: phase transition due to the combined effect of the functionalization compound and particle size. J Appl Phys. 2009;105:084305.

[40] Darling SB. Directing the self-assembly of block copolymers. Prog Polym Sci. 2007;32:1152–1204.

[41] Patti A. Molecular dynamics of spherical nanoparticles in dense polymer melts. J Phys Chem B. 2014;118:3731–3742.

[42] Lamarre SS, Lemay C, Labrecque C, et al. Controlled 2D organization of gold nanoparticles in block copolymer monolayers. Langmuir. 2013;29:10891–10898.

[43] Ledo-Suarez A, Hoppe CE, Lazzari M, et al. Thermal annealing as an easy tool for the controlled arrangement of gold nanoparticles in block-copolymer thin films. Nanotechnology. 2013;24:255304.

[44] Jayaraman A. Polymer grafted nanoparticles: effect of chemical and physical heterogeneity in polymer grafts on particle assembly and dispersion. J Polym Sci Part B Polym Phys. 2013;51:524–534.

[45] Zhang T, Cong Y, Zhang B, et al. Preparation and characterisation: PSCLC film doping with FexNiy nanoparticles. Liq Cryst. 2015;42:167–173.

[46] Ten Brinke G, Ruokolainen J, Ikkala O. Supramolecular materials based on hydrogen-bonded polymers. Hydrogen Bonded Polym. 2007;207:113–177.

[47] Long Y, Hui JF, Wang PP, et al. Hydrogen bond nanoscale networks showing switchable transport performance. Sci Rep. 2012;2:612.

[48] De Feyter S, Miura A, Yao S, et al. Two-dimensional self-assembly into multicomponent hydrogen-bonded nanostructures. Nano Lett. 2005;5:77–81.

[49] Ciesielski A, Szabelski PJ, Rzysko W, et al. Concentration-dependent supramolecular engineering of hydrogen-bonded nanostructures at surfaces: predicting self-assembly in 2D. J Am Chem Soc. 2013;135:6942–6950.

[50] Soto-Bustamante EA, Beresnev LA, Blinov LM, et al., inventor; Deutsche Telekom Ag, assignee. Methode zur Herstellung von polymeren pyroelektrischen und piezoelektrischen Elementen.Germany patent DE19547934 20 Dic 1995.

[51] Kasch N, Dierking I, Turner M, et al. Liquid crystalline textures and polymer morphologies resulting from electropolymerisation in liquid crystal phases. J Mater Chem C. 2015;3:8018–8023.

[52] Meneses-Franco A, Fierro-Armijo AE, Romero-Hasler P, et al. Smectogenic liquid crystals and nanoparticles: an approach for potential application in photovoltaics. J Mater Chem C. 2015;3:8566–8573.

[53] Soto-Bustamante EA, Haase W. Synthesis of new liquid crystalline monomers for nonlinear optics X-ray study of reentrant nematic behaviour with smectic-like fluctuations of c type. Liq Cryst. 1997;23:603–612.

[54] Soto-Bustamante EA, Galyametdinov YG, Griesar K, et al. Synthesis and characterization of a novel liquid crystalline side chain metallopolymer. Macromol Chem Phys. 1998;199:1337–1342.

[55] Soto-Bustamante EA, Saldaño-Hurtado D, Vergara-Toloza RO, et al. Phase characterization of two homologous series of LC methacrylic monomers based on w-hexyl- and w-butyloxysalicylaldimine group with different alkoxy tail substitutions. Liq Cryst. 2003;30:17–22.

[56] Blanton TN, Huang TC, Toraya H, et al. JCPDS - international centre for diffraction data round robin study of silver behenate. A possible low-angle X-ray diffraction calibration standard. Powder Diffr. 1995;10:91–95.

[57] Martinez-Miranda LJ, Taylor JW, Kurihara LK. Interfacial structure of a liquid crystal/nanoparticle nanocomposite studied by X-ray scattering: indirect evidence for the role of faceting of the nanoparticles. Langmuir. 2016;32:239–246.

[58] Martinez-Miranda LJ. Smectic ordering in confined liquid crystal films: A depth study. J Appl Phys. 2002;91:6452–6456.

[59] Wang J, Watson GM, Ocko BM. Uniaxial incommensurate phases at the Au(111) electrode. Physica A. 1993;200:679–687.

[60] Shandryuk GA, Matukhina EV, Vasil'ev RB, et al. Effect of H-bonded liquid crystal polymers on CdSe quantum dot alignment within nanocomposite. Macromolecules. 2008;41:2178–2185.